PROCEEDINGS of the
23rd International Congress on Acoustics
9 to 13 September 2019 in Aachen, Germany

2.5D Local wave field synthesis of a virtual plane wave using a time domain representation of spherical harmonics expansion

Nara HAHN; Fiete WINTER; Sascha SPORS

Institute of Communications Engineering
University of Rostock, Rostock, Germany
nara.hahn@uni-rostock.de

ABSTRACT

Wave field synthesis is a well established sound reproduction technique, where the wavefront of a desired sound field is physically recreated within an extended target area by using a large number of individually driven loudspeakers. For a non-continuous loudspeaker distribution, the synthesized sound field typically exhibits spatial aliasing artifacts which occur above an upper frequency limit. If the synthesis in a relatively small area is concerned, called local wave field synthesis, the physical accuracy of the sound field can be improved significantly. This was achieved in a recently proposed method, where the target sound field is expanded into a finite number of cylindrical harmonic components with respect to a properly chosen expansion center. The present paper deals with the time domain realization of this method for a 2.5-dimensional setup. The driving function for a virtual plane wave is derived based on the time domain version of the spherical harmonics expansion. Due to the low computational cost, the proposed approach is well suited for real-time implementation. The spatial, temporal, and spectral properties of the synthesized sound fields are evaluated by numerical simulations.

Keywords: local wave field synthesis, spherical harmonics expansion, time domain

1 INTRODUCTION

Wave Field Synthesis (WFS), sometimes called wavefront synthesis, is a sound field synthesis method which is based on the high frequency approximation of the Kirchhoff-Helmholtz integral equation [1, 2]. While the high spatial fidelity of WFS is consistently supported by listening experiments [3–6], the timbral degradation is still a challenge [7, 8]. This is mainly attributed to the discrete distribution of secondary sources, which causes spectral distortions, called spatial aliasing artifacts. The artifacts are pronounced at high frequencies, where, roughly speaking, the half wavelength is smaller than the distance between the loudspeakers. Unless a continuous (or at least quasi-continuous in a practical sense) loudspeaker array is developed, spatial aliasing is inevitable and should be accepted as a physical limitation.

Although the spatial aliasing artifacts cannot be removed completely, it is possible to spatially redistribute them in a controlled way. If the requirement for an accurate synthesis is relaxed to a smaller area, the performance can be improved at the expanse of stronger artifacts occurring elsewhere. Such a technique is called local WFS and a couple of methods were proposed in the past years [9–11]. The present study focuses on the method using spatial band limitation [11], where the target sound field is expanded in terms of spherical/cylindrical harmonics with respect to the target position, and the size of the aliasing-free area is controlled by varying the maximum order of the expansion. The driving function of this method was initially derived in the temporal frequency domain, which demands intense computations due to the evaluation of the Bessel functions at all frequency bins. Two time domain realizations are introduced in [12, 13], one of which exploits the time domain representation of the cylindrical harmonics expansion [13]. While it exhibits significantly lower computations, some tweaks are needed to cope with temporal aliasing and excessive amplitude.

In this paper, an improved version of the time domain driving function is proposed for local WFS. The proposed driving function is derived in Sec. 2. The so called 2.5-dimensional (2.5D) setup is considered, meaning that a 2D target sound field is synthesized by means of secondary point sources distributed in the horizontal plane. Similar to [13], the target sound field is initially described in terms of cylindrical harmonics with a limited spatial bandwidth, i.e. finite number of cylindrical harmonics. The spatial windowing associated with the directional gradient and secondary source selection is performed in the cylindrical harmonics domain, and the resulting coefficient is converted into the spherical harmonics domain, followed by amplitude correction and equalization. In Sec. 3, the proposed driving function is used in numerical simulations in order to evaluate the accuracy of the synthesized sound fields. The paper closes with a brief conclusion in Sec. 4.

1.1 Nomenclature

The following notational conventions are used throughout this paper. Frequency domain sound fields are denoted by uppercase $S(\boldsymbol{x}, \omega)$ and time domain sound fields by lowercase $s(\boldsymbol{x}, t)$, where $\omega = 2\pi f$ denotes the angular frequency and t the time. Position vectors $\boldsymbol{x} = (r, \theta, \phi)$ are denoted by lowercase boldface. Unless stated otherwise, the spherical coordinates are used, where θ denotes the colatitude and ϕ the azimuth. A scalar product of two vectors is denoted by $\langle \cdot, \cdot \rangle$. The imaginary unit is denoted by i and the speed of sound by c.
The cylindrical harmonics expansion of a 2D interior sound field reads [14, Eq. (4.49)]

$$S(\boldsymbol{x}, \omega) = \sum_{m=-\infty}^{\infty} \mathring{S}_m(\omega)\, i^{-m} J_m(\tfrac{\omega}{c} r \sin\theta)\, e^{im\phi}, \tag{1}$$

where $J_m(\cdot)$ denotes the cylindrical Bessel function of the first kind, and $\mathring{S}_m(\omega)$ the expansion coefficient. The spherical harmonics expansion of an interior sound field reads [14, Eq. (6.21)]

$$S(\boldsymbol{x}, \omega) = \sum_{n=0}^{\infty} \sum_{m=-n}^{n} \breve{S}_{nm}(\omega)\, i^{-n} j_n(\tfrac{\omega}{c} r)\, Y_{nm}(\theta, \phi) \tag{2}$$

where $j_n(\cdot)$ denotes the spherical Bessel function of the first kind, and $\breve{S}_{nm}(\omega)$ the expansion coefficient. The spherical harmonic of degree n and order m is defined as

$$Y_{nm}(\theta, \phi) = \sqrt{\tfrac{2n+1}{4\pi} \tfrac{(n-m)!}{(n+m)!}}\, P_n^m(\cos\theta) e^{im\phi}, \tag{3}$$

where $P_n^m(\cdot)$ denotes the associated Legendre polynomial.

2 DRIVING FUNCTIONS

2.1 Conventional WFS

The conventional 2.5D driving function for a virtual plane wave propagating in the direction $\boldsymbol{n}_{\text{pw}} = (1, \frac{\pi}{2}, \phi_{\text{pw}})$ reads [15, Eq. (2.177)]

$$D_{\text{WFS}}(\boldsymbol{x}_0, \omega) = \sqrt{8\pi \|\boldsymbol{x}_{\text{ref}} - \boldsymbol{x}_0\|} \sqrt{i\tfrac{\omega}{c}} \underbrace{\max\{\langle \boldsymbol{n}_{\text{pw}}, \boldsymbol{n}_0(\boldsymbol{x}_0) \rangle, 0\}}_{a(\boldsymbol{x}_0)} e^{-i\frac{\omega}{c}\langle \boldsymbol{n}_{\text{pw}}, \boldsymbol{x} \rangle} \tag{4}$$

in the frequency domain, and [15, Eq. (2.178)]

$$d_{\text{WFS}}(\boldsymbol{x}_0, t) = \sqrt{8\pi \|\boldsymbol{x}_{\text{ref}} - \boldsymbol{x}_0\|}\, h(t) *_t a(\boldsymbol{x}_0)\, \delta\big(t - \tfrac{\langle \boldsymbol{n}_{\text{pw}}, \boldsymbol{x} \rangle}{c}\big) \tag{5}$$

in the time domain, where $\delta(t)$ denotes the Dirac delta function and $*_t$ the convolution in the time domain. The position of the secondary sources is denoted by $\boldsymbol{x}_0 = (r_0, \frac{\pi}{2}, \phi_0)$, and the inward surface normal vector at $\boldsymbol{x}_0$ by

$\boldsymbol{n}_0(\boldsymbol{x}_0) = (1, \frac{\pi}{2}, \phi_{\boldsymbol{n}_0})$. The amplitude errors occurring in 2.5D configurations can be corrected by $\sqrt{\|\boldsymbol{x}_{\text{ref}} - \boldsymbol{x}_0\|}$ for a reference position $\boldsymbol{x}_{\text{ref}}$. Compensating the dimensionality mismatch between the 2D sound field and the 3D secondary sources (point sources) also requires the equalization $\sqrt{i\frac{\omega}{c}}$ which exhibits a slope of $+3$ dB/octave and a constant phase of $\frac{\pi}{4}$. In the time domain, this is performed by the filter $h(t) = \mathcal{F}^{-1}\{\sqrt{i\frac{\omega}{c}}\}$. The spatial window $a(\boldsymbol{x}_0)$ is a rectified cosine function which activates the secondary sources only if $\langle \boldsymbol{n}_{\text{pw}}, \boldsymbol{n}_0(\boldsymbol{x}_0)\rangle > 0$. It also applies a cosine weight $\langle \boldsymbol{n}_{\text{pw}}, \boldsymbol{n}_0(\boldsymbol{x}_0)\rangle > 0$ which comes from the direction gradient of the sound field. The interested readers are referred to [2, 15] for more detailed treatments.

2.2 Local WFS

For local WFS of a plane wave, a spatial band limitation is applied to the sound field in the cylindrical harmonics domain. In the horizontal plane ($\theta = \frac{\pi}{2}$), this reads [16, Sec. 2.6]

$$S(\boldsymbol{x}, \omega) = \sum_{m=-M}^{M} \underbrace{e^{-im\phi_{\text{pw}}}}_{\mathring{S}_m(\phi_{\text{pw}})} i^{-m} J_m(\tfrac{\omega}{c} r) e^{im\phi}, \tag{6}$$

where M denotes the spatial bandwidth of the expansion. Notice that the coefficient $\mathring{S}_m(\phi_{\text{pw}}) = e^{-im\phi_{\text{pw}}}$ also describes the 2D plane wave expansion of the sound field [16, Sec. 2.6],

$$S(\boldsymbol{x}, \omega) = \int_0^{2\pi} \underbrace{\sum_{m=-M}^{M} \mathring{S}_m(\phi_{\text{pw}}) e^{im\bar{\phi}}}_{\bar{S}(\bar{\phi})} e^{-i\frac{\omega}{c} r \cos(\phi - \bar{\phi})} \mathrm{d}\bar{\phi}, \tag{7}$$

where the sound field is represented as a superposition of plane waves. The direction of the individual plane waves is denoted by $\bar{\boldsymbol{n}} = (1, \bar{\theta}, \bar{\phi})$ and the corresponding amplitude by $\bar{S}(\bar{\phi})$. A spatial band limitation constitutes a rectangular windowing of $\mathring{S}_m(\omega)$ in the m domain, which corresponds to a circular convolution with a periodic sinc function in the $\bar{\phi}$ domain. For a single plane wave, i.e. $\bar{S}(\bar{\phi}) = \delta(\bar{\phi} - \phi_{\text{pw}})$, a spatial band limitation smears the spatial structure of the sound field.

For a given secondary source position $\boldsymbol{x}_0$, the spatial window

$$a(\boldsymbol{x}_0) = \max\{\langle \bar{\boldsymbol{n}}, \boldsymbol{n}_0(\boldsymbol{x}_0)\rangle, 0\} \tag{8}$$

has to be applied to every plane wave in (7). The window function can be approximated as a truncated Fourier series expansion (equivalent to cylindrical harmonics expansion),

$$a(\boldsymbol{x}_0) \approx \sum_{m=-M_a}^{M_a} \mathring{a}_m(\phi_{\boldsymbol{n}_0})\, e^{im\bar{\phi}}, \tag{9}$$

where M_a denotes the modal bandwidth and $\mathring{a}_m(\phi_{\boldsymbol{n}_0})$ the Fourier coefficients,

$$\mathring{a}_m = \frac{1}{2\pi} \int_{-\pi}^{\pi} a(\boldsymbol{x}_0)\, e^{-im\bar{\phi}} \mathrm{d}\bar{\phi} = \begin{cases} \dfrac{(-1)^{m/2}}{\pi(1-m^2)} e^{-im\phi_{\boldsymbol{n}_0}}, & m \text{ even} \\ \dfrac{1}{4} e^{-im\phi_{\boldsymbol{n}_0}}, & m = \pm 1 \\ 0, & \text{else.} \end{cases} \tag{10}$$

The spatial windowing is performed in the cylindrical harmonic domain which constitutes a convolution (denoted by $*_m$) of the coefficients,

$$\mathring{D}_m(\phi_{\text{pw}}, \phi_{\boldsymbol{n}_0}) = \mathring{S}_m(\phi_{\text{pw}}) *_m \mathring{a}_m(\phi_{\boldsymbol{n}_0}) \coloneqq \sum_{\mu=\mu_{\min}}^{\mu_{\max}} \mathring{S}_\mu(\phi_{\text{pw}})\, \mathring{a}_{m-\mu}(\phi_{\boldsymbol{n}_0}), \quad m = -(M + M_a), \ldots, (M + M_a), \tag{11}$$

where $\mu_{\text{min}} = \max\{-M, -M_a + m\}$ and $\mu_{\text{max}} = \min\{M, M_a + m\}$. The coefficient $\mathring{D}_m(\phi_{\text{pw}}, \phi_{\boldsymbol{n}_0})$ exhibits a spatial bandwidth of $M_d = M + M_a$. Notice that $\mathring{D}_m(\phi_{\text{pw}}, \phi_{\boldsymbol{n}_0})$ describes the spatially windowed version of the sound field which corresponds to the last two terms in the right-hand side of (4) or (5). The amplitude correction and equalization are not applied yet.

At this point, $\mathring{D}_m(\phi_{\text{pw}}, \phi_{\boldsymbol{n}_0})$ can be used to represent the driving function as a 2D plane wave expansion or equivalently as a cylindrical harmonics expansion. However, as discussed in [13], the analytical time domain modeling of the radial function $J_m(\frac{\omega}{c}r)$ causes temporal aliasing which requires some heuristic adjustments. In the present work, this is avoided by replacing the cylindrical harmonics expansion with a spherical harmonics expansion. For 2D sound fields, the coefficient can be converted as [17, Eq. (14)]

$$\breve{D}_{nm}(\phi_{\text{pw}}, \phi_{\boldsymbol{n}_0}) = 4\pi Y^*_{nm}(\tfrac{\pi}{2}, 0)\, \mathring{D}_m(\phi_{\text{pw}}, \phi_{\boldsymbol{n}_0}). \tag{12}$$

Note that, an additional term i^{m-n} is present in [17, Eq. (14)], as the definition of the coefficients is slightly different. The resulting spherical harmonics expansion reads

$$\tilde{D}(\boldsymbol{x}_0, \omega) = \sum_{m=-M_d}^{M_d} \sum_{n=|m|}^{\infty} 4\pi\, Y^*_{nm}(\tfrac{\pi}{2}, 0)\, \mathring{D}_m(\phi_{\text{pw}}, \phi_{\boldsymbol{n}_0})\, i^{-n} j_n(\tfrac{\omega}{c} r_0)\, Y_{nm}(\tfrac{\pi}{2}, \phi_0) \tag{13}$$

$$\approx \sum_{m=-M_d}^{M_d} \sum_{n=|m|}^{N} 4\pi\, Y^*_{nm}(\tfrac{\pi}{2}, 0)\, \mathring{D}_m(\phi_{\text{pw}}, \phi_{\boldsymbol{n}_0})\, i^{-n} j_n(\tfrac{\omega}{c} r_0)\, Y_{nm}(\tfrac{\pi}{2}, \phi_0). \tag{14}$$

While (13) is equivalent to the cylindrical harmonics expansion, (14) is an approximation of the former where the degree n is truncated to N. The radial part is now described by spherical Bessel functions $j_n(\frac{\omega}{c}r_0)$ which exhibit a strong roll-off at high frequencies, therefore, the time discretization causes significantly less temporal aliasing.

The only frequency dependent term in (14) is $j_n(\frac{\omega}{c}r_0)$ whose inverse Fourier transform reads [18, Eq. (10.59.1)]

$$\mathcal{F}^{-1}\{i^{-n} j_n(\tfrac{\omega}{c} r_0)\} = \tfrac{c}{2r_0} P_n(\tfrac{ct}{r_0}), \tag{15}$$

with $P_n(\cdot)$ denoting the Legendre polynomial. The time domain representation of the spherical harmonics expansion thus reads [19]

$$\tilde{d}(\boldsymbol{x}_0, t) = \frac{c}{2r_0} \sum_{nm}^{NM_d} 4\pi Y^*_{nm}(\tfrac{\pi}{2}, 0) \mathcal{F}^{-1}\{\mathring{D}_m(\phi_{\text{pw}}, \phi_{\boldsymbol{n}_0})\} *_t P_n(\tfrac{ct}{r_0})\, Y_{nm}(\tfrac{\pi}{2}, \phi_0) \tag{16}$$

$$= \frac{c}{2r_0} \sum_{nm}^{NM_d} 4\pi Y^*_{nm}(\tfrac{\pi}{2}, 0) \mathring{D}_m(\phi_{\text{pw}}, \phi_{\boldsymbol{n}_0}) P_n(\tfrac{ct}{r_0})\, Y_{nm}(\tfrac{\pi}{2}, \phi_0) \tag{17}$$

$$= \frac{c}{2r_0} \sum_{nm}^{NM_d} (2n+1) P_n(\tfrac{ct}{r_0}) \mathring{D}_m(\phi_{\text{pw}}, \phi_{\boldsymbol{n}_0}) K_n^m e^{im\phi_0}, \tag{18}$$

where a shorthand notation is used for the double summation, $\sum_{nm}^{NM_d} := \sum_{m=-M_d}^{M_d} \sum_{n=|m|}^{N}$. The frequency independence of $\breve{D}_{nm}(\phi_{\text{pw}}, \phi_{\boldsymbol{n}_0})$ is exploited in the second equality, i.e.

$$\mathcal{F}^{-1}\{\mathring{D}_m(\phi_{\text{pw}}, \phi_{\boldsymbol{n}_0})\} = \mathring{D}_m(\phi_{\text{pw}}, \phi_{\boldsymbol{n}_0}) \cdot \delta(t).$$

The coefficient K_n^m in the third equality is defined as [20, p. 783]

$$K_n^m := \tfrac{(n-m)!}{(n+m)!} \big(P_n^m(0)\big)^2 = \begin{cases} \frac{(n-m-1)!!(n+m-1)!!}{(n+m)!!(n-m)!!}, & n+m \text{ even} \\ 0, & n+m \text{ odd}, \end{cases} \tag{19}$$

with $(\cdot)!!$ denoting the double factorial. It can be computed efficiently by exploiting $K_0^0 = 1$ and the recurrence relations,

$$K_n^m = \tfrac{n+m-1}{n+m} K_{n-1}^{m-1}, \qquad K_n^m = \tfrac{n-m-1}{n-m} K_{n-1}^{m+1}. \tag{20}$$

Notice from (19) that the spherical harmonics expansion of a 2D sound field requires only the coefficients with even $n+m$. Finally, the time domain driving function is obtained by multiplying the amplitude correction factor and applying the equalization filter (cf. (5)),

$$d_{\text{LWFS}}(\boldsymbol{x}_0, t) = \sqrt{8\pi \|\boldsymbol{x}_{\text{ref}} - \boldsymbol{x}_0\|}\, h(t) *_t \frac{c}{2r_0} \sum_{nm}^{NM_d} (2n+1) P_n(\tfrac{ct}{r_0})\, \mathring{D}_m(\phi_{\text{pw}}, \phi_{\boldsymbol{n}_0})\, K_n^m e^{im\phi_0}. \tag{21}$$

Once the target position $\boldsymbol{x}_{\text{ref}}$ is determined, the coordinate system can be translated so that it coincides with the origin, i.e. $\boldsymbol{x}' = \boldsymbol{x} - \boldsymbol{x}_{\text{ref}}$. The driving function is then simplified as

$$d_{\text{LWFS}}(\boldsymbol{x}_0', t) = c \sqrt{\frac{2\pi}{r_0'}}\, h(t) *_t \sum_{nm}^{NM_d} (2n+1) P_n(\tfrac{ct}{r_0'})\, \mathring{D}_m(\phi_{\text{pw}}, \phi_{\boldsymbol{n}_0})\, K_n^m\, e^{im\phi_0'}, \tag{22}$$

where $\boldsymbol{x}_0' = \boldsymbol{x}_0 - \boldsymbol{x}_{\text{ref}} = (r_0', \frac{\pi}{2}, \phi_0')$ denotes the secondary source position in the new coordinate system.

3 EVALUATION

The local synthesis of a virtual plane wave is simulated by using the proposed driving function (22). A total of 60 ideal secondary point sources are uniformly distributed on a circle with radius of 1.5 m (spacing of 15.7 cm). The virtual plane wave propagates in the $-y$ direction, i.e. $\boldsymbol{n}_{\text{pw}} = (1, \frac{\pi}{2}, -\frac{\pi}{2})$. Four different target positions (x, y, z) are chosen, where the spatial aliasing artifacts should be suppressed:

$$\text{‘Center’} : (0,0,0), \quad \text{‘Right’} : (0.75,0,0), \quad \text{‘Front’} : (0,0.75,0), \quad \text{‘Back’} : (0,-0.75,0).$$

In each case, the target position is used as the expansion center of the driving function. While the spatial bandwidth of the sound field is varied $M = 15, 23$, a fixed bandwidth $M_a = 20$ is used for the spatial window $a(\boldsymbol{x}_0)$. The maximum order of the spherical harmonics expansion is thus $M_d = M + M_a = 35, 43$, and the maximum degree n is set equal to the maximum order $N = M_d$. The discrete-time driving function is obtained by sampling (22) at integer multiples of the sampling interval. A max-$\boldsymbol{r}_E$ window is applied to the driving function [21, Eq. (10)]. The simulations are performed at a sampling rate of $f_s = 88.2$ kHz, but the frequency responses are evaluated only for audio band $f \leq 22$ kHz. The pre-equalization filter is realized as a linear phase FIR filter (513 taps), therefore the constant phase $\frac{\pi}{4}$ is omitted. The speed of sound is set to $c = 343$ m/s.

The driving functions are shown in Fig 1, where the equalization filter is not applied to better visualize the temporal structure. The first thing to notice is the high amplitude pulses along the curve $t = \frac{r_0}{c}\cos(\phi_0 - \phi_{\text{pw}})$ for $\phi_0 \in [0, \pi)$, which is almost independent to the target positions. This shows that, in the low frequencies, the local WFS driving function coincides with the conventional one (5). The fine structure of the driving functions, representing the high frequency components, depends on the target position with varying spatial and temporal characteristics. The non-causality of the driving functions is due to the definition of the plane wave which passes the origin at time $t = 0$. In practice, a pre-delay has to be added.

The synthesized sound fields on the xy-plane are visualized in Fig. 2. At each target position (indicated by ‘+’), a strong impulse is received which corresponds to the wavefront of the virtual plane wave. In the bottom row, the driving functions are band limited in the temporal frequency domain, as indicated at the top-left corner of each plot. For a bandwidth of 500 Hz (leftmost), the wavefront is almost perfectly synthesized within the entire area surrounded by the loudspeakers. A phase distortion can be seen which is due to the linear phase design of the equalization filter $h(t)$. As the temporal bandwidth increases, the synthesis is correct only within

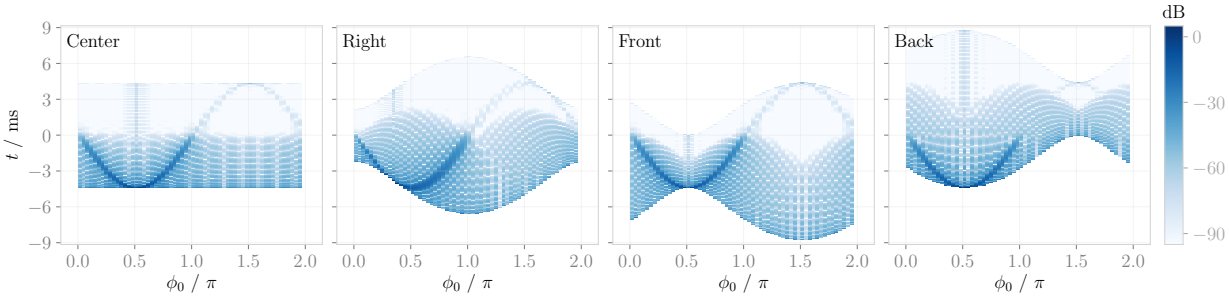

Figure 1. Proposed local WFS driving functions ($\phi_{\text{pw}} = -\frac{\pi}{2}$, $M = 23$, max-$\boldsymbol{r}_E$ window, without equalization).

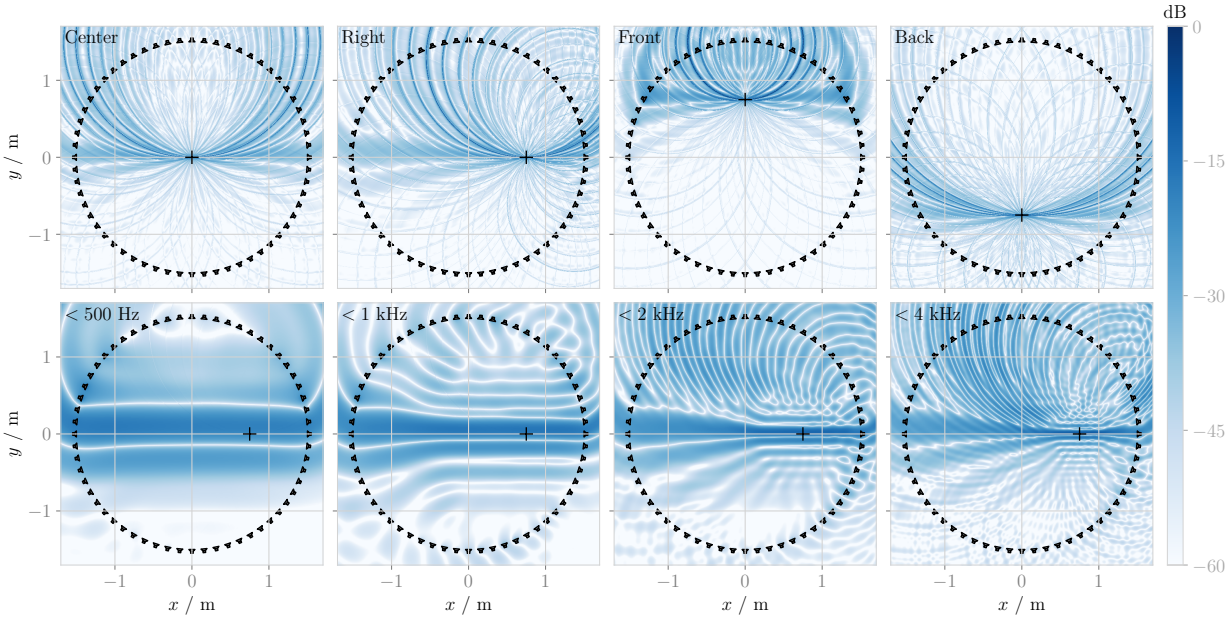

Figure 2. Synthesized sound fields ($\phi_{\text{pw}} = -\frac{\pi}{2}$, $M = 23$, max-$\boldsymbol{r}_E$ window). Top: full-band sound fields for different target positions. Bottom: temporally band limited sound fields for target position 'Right'. The secondary point sources are indicated by the loudspeaker symbols and the target positions by '+'.

a circular area, the radius of which scales down. For the rest of the listening area, the wavefront is smeared and sound waves propagating in wrong directions are superimposed. The former is due to spatial band limitation whereas the latter is caused by spatial aliasing.

The received time signals at the target positions are shown in Fig. 3a (left). The phase distortion mentioned above is clearly seen. In Fig. 3a (right), the impulse responses at the same receiver positions are evaluated, but the driving function for the target position 'Right' is used. The temporal smearing can be seen at off-target positions.

In Fig. 3b, the frequency responses at the target positions are depicted by coloured lines. Above 300 Hz, the magnitude responses are almost flat with moderate fluctuations (< 3 dB). The roll-off in the lower end is attributed to the high-frequency approximation employed in WFS. Since the low frequency deviations are almost constant, the overall system response can be equalized, e.g. by a shelving filter. The spectral variations around the target positions are also evaluated, which might occur due to listener's movements or head rotations.

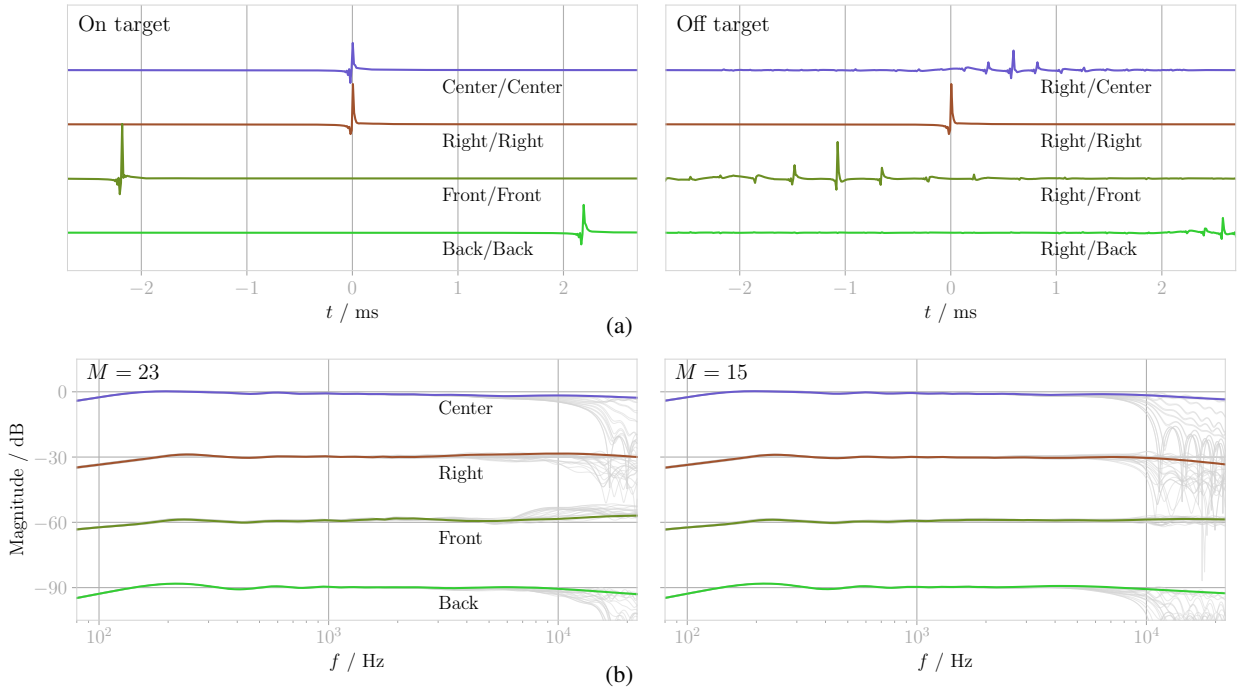

Figure 3. (a) Impulse responses ($M = 23$) for different target/receiver positions. (b) Frequency responses ($M = 23, 15$) at on- and off-target positions. The thin gray curves show the frequency responses on a circle centered at each target position (radius of 8.5 cm, 20 uniform angles).

Twenty equiangular points are chosen on a circle with radius 8.5 cm centred at each target position. The radius corresponds to the half wavelength of 2 kHz. The frequency responses at those positions are plotted with thin gray curves in Fig. 3b. High frequency (> 5 kHz) attenuation is observed in most cases, which is a typical effect of a spatial band limitation. However, in Fig. 3b (left, $M = 23$), the frequency responses around 'Front' exhibit high frequency boost which is caused by spatial aliasing. This agrees with the observation in [22], that the spatial aliasing is more pronounced at positions those are closer to the virtual sound source. The influence of spatial aliasing can be reduced to some extent by decreasing the spatial bandwidth. As shown in 3b (right), the spectral distortion at 'Front' is significantly reduced, but the high frequency attenuation at other target positions becomes more severe. The spatial bandwidth has to be chosen in such a way that the spectral distortion due to the spatial band limitation and the spatial aliasing artifacts are in an acceptable level within the listening area. Alternatively, the spatial bandwidth can be adaptively changed according to the tracked listener position. It can benefit from a geometric prediction model of spatial aliasing artifacts, such as [22].

4 CONCLUSION

In this paper, a time domain driving function for local WFS was introduced which is represented as a spherical harmonics expansion. The significant reduction of spatial aliasing around the target positions is demonstrated by numerical simulations The size of the aliasing-free area can be controlled by varying the spatial bandwidth. No noticeable artifact due to temporal aliasing is found which was problematic in the earlier approach [13]. The computational efficiency is still maintained, due to the recurrence relation of the coefficients. This makes the proposed method suited for real time and dynamic scenarios, where the listener movements are tracked and the driving functions are updated accordingly.

REFERENCES

[1] A. J. Berkhout, D. de Vries, and P. Vogel, "Acoustic Control by Wave Field Synthesis," *J. Acoust. Soc. Am. (JASA)*, vol. 93, no. 5, pp. 2764–2778, 1993.

[2] S. Spors, R. Rabenstein, and J. Ahrens, "The Theory of Wave Field Synthesis Revisited," in *Proc. 124th Audio Eng. Soc. (AES) Conv.*, 2008.

[3] H. Wierstorf, *Perceptual Assessment of Sound Field Synthesis*. Doctoral thesis, Technical University of Berlin, 2014.

[4] P. Vogel, *Application of Wave Field Synthesis in Room Acoustics*. PhD thesis, Delft University of Technology, 1995.

[5] E. Verheijen, *Sound Reproduction by Wave Field Synthesis*. PhD thesis, Delft University of Technology, 1997.

[6] E. W. Start, *Direct Sound Enhancement by Wave Field Synthesis*. PhD thesis, Delft University of Technology, 1997.

[7] H. Wierstorf, C. Hohnerlein, S. Spors, and A. Raake, "Coloration in Wave Field Synthesis," in *Proc. 55th Audio Eng. Soc. (AES) Int. Conf. Spatial Audio*, Audio Engineering Society, 2014.

[8] H. Wittek, *Perceptual Differences between Wavefield Synthesis and Stereophony*. PhD thesis, University of Surrey Surrey, UK, 2007.

[9] S. Spors and J. Ahrens, "Local Sound Field Synthesis by Virtual Secondary Sources," in *Proc. 40th Audio Eng. Soc. (AES) Int. Conf. Spatial Audio*, (Tokyo, Japan), Oct. 2010.

[10] S. Spors, K. Helwani, and J. Ahrens, "Local Sound Field Synthesis by Virtual Acoustic Scattering and Time-reversal," in *Proc. 131th Audio Eng. Soc. (AES) Conv.*, (New York, USA), Oct. 2011.

[11] N. Hahn, F. Winter, and S. Spors, "Local Wave Field Synthesis by Spatial Band-limitation in the Circular/Spherical Harmonics Domain," in *Proc. 140th Audio Eng. Soc. (AES) Conv.*, (Paris, France), June 2016.

[12] F. Winter, N. Hahn, and S. Spors, "Time-Domain Realisation of Model-Based Rendering for 2.5D Local Wave Field Synthesis Using Spatial Bandwidth-Limitation," in *Proc. Eur. Signal Process. Conf. (EUSIPCO)*, (Kos, Greece), 2017.

[13] N. Hahn, F. Winter, and S. Spors, "Synthesis of a Spatially Band-Limited Plane Wave in the Time-Domain Using Wave Field Synthesis," in *Proc. Eur. Signal Process. Conf. (EUSIPCO)*, (Kos, Greece), 2017.

[14] E. G. Williams, *Fourier Acoustics: Sound Radiation and Nearfield Acoustical Holography*. Academic press, 1999.

[15] F. Schultz, *Sound Field Synthesis for Line Source Array Applications in Large-Scale Sound Reinforcement*. Doctoral thesis, University of Rostock, 2016.

[16] A. Kuntz, *Wave Field Analysis using Virtual Circular Microphone Arrays*. Verlag Dr. Hut, 2008.

[17] N. Hahn and S. Spors, "Sound Field Synthesis of Virtual Cylindrical Waves using Circular and Spherical Loudspeaker Arrays," in *Proc. 138th Audio Eng. Soc. (AES) Conv.*, Audio Engineering Society, 2015.

[18] F. W. Olver, D. W. Lozier, R. F. Boisvert, and C. W. Clark, *NIST Handbook of Mathematical Functions Handback*. Cambridge University Press, 2010.

[19] N. Hahn and S. Spors, "Time-Domain Representations of a Plane Wave with Spatial Band-Limitation in the Spherical Harmonics Domain," in *Proc. 45th German Annu. Conf. Acoust. (DAGA)*, (Rostock, Germany), Mar. 2019.

[20] G. B. Arfken and H. J. Weber, *Mathematical Methods for Physicists*. Academic press, 2005.

[21] F. Zotter and M. Frank, "All-Round Ambisonic Panning and Decoding," *J. Audio Eng. Soc*, vol. 60, no. 10, pp. 807–820, 2012.

[22] F. Winter, F. Schultz, G. Firtha, and S. Spors, "A Geometric Model for Prediction of Spatial Aliasing in 2.5D Sound Field Synthesis," *IEEE/ACM Trans. Audio, Speech, and Language Process.*, vol. 27, pp. 1031–1046, June 2019.